Eur. Phys. J. A (2016) **52**: 368
DOI 10.1140/epja/i2016-16368-6

THE EUROPEAN PHYSICAL JOURNAL A

Regular Article – Theoretical Physics

Fourier transforms of single-particle wave functions in cylindrical coordinates

M. Rizea[1,a] and N. Carjan[1,2,3]

[1] National Institute of Physics and Nuclear Engineering, "Horia Hulubei", PO Box MG-6, Bucharest, Romania
[2] Joint Institute for Nuclear Research, FLNR, 141980 Dubna, Moscow Region, Russia
[3] CENBG, University of Bordeaux, 33175 Gradignan Cedex, France

Received: 6 October 2016 / Revised: 12 December 2016
Published online: 27 December 2016 –
Communicated by F. Gulminelli

Abstract. A formalism and the corresponding numerical procedures that calculate the Fourier transform of a single-particle wave function defined on a grid of cylindrical (ρ, z) coordinates is presented. Single-particle states in spherical and deformed nuclei have been chosen in view of future applications in the field of nuclear reactions. Bidimensional plots of the probability that the nucleon's momentum has a given value $K = \sqrt{k_\rho^2 + k_z^2}$ are produced and from them the K-distributions are deduced. Three potentials have been investigated: a) a sharp surface spherical well (*i.e.*, of constant depth), b) a spherical Woods-Saxon potential *i.e.*, diffuse surface) and c) a deformed potential of Woods-Saxon type. In the first case the momenta are as well defined as allowed by the uncertainty principle. Depending on the state, their distributions have up to three separated peaks as a consequence of the up to three circular ridges of the bidimensional probabilities plots. In the second case the diffuseness allows very low momenta to be always populated thus creating tails towards the origin ($K = 0$). The peaks are still present but not well separated. In the third case the deformation transforms the above mentioned circular ridges into ellipses thus spreading the K-values along them. As a consequence the K-distributions have only one broad peak.

1 Introduction

In many nuclear physics applications it is necessary to know the momentum distribution associated with a given wave function and therefore its Fourier transform is needed. For instance, the calculation of the Fourier transform (FT) of a single-particle wave function (WF) is required in theoretical approaches of direct nuclear reactions of stripping, pick-up and knock-out types [1–3]. In particular, the FTs of the WFs of the bound nucleons in the entrance and exit channels are essential ingredients in the expression of the stripping and pick-up reaction amplitudes, hence of the cross section. They represent the momentum transfers that occur during the reaction and give the probability that such an event takes place. Likewise, the knock-out cross section and the parallel momentum distribution of the ejected nucleon are computed from the FT of the corresponding WF.

With the recent development of radioactive ion beam facilities, the field of direct nuclear reactions has been revisited and provides at present the most sensitive tools for the spectroscopy of nuclei far from stability. Although the nuclei involved in these reactions are often deformed, the calculations have been performed in spherical coordinates neglecting the, undoubtedly important, role of the deformation. This is mainly because a deformed WF is commonly expressed in cylindrical coordinates and the procedure to calculate its FT is quite complicated. The purpose of the present paper is to raise this challenge: develop a formalism, an algorithm and the associated computer program that allows to calculate the FT of a WF that is given in cylindrical (ρ, z) coordinates. It is the first endeavour of this kind.

Another application of the FT of a WF in extremely deformed nuclei is in the field of nuclear fission. The momentum distribution of the scission neutrons (those that are emitted during the neck rupture) is given by the FT of the tail of their wave packets that is in the continuum [4]. From the momentum distribution one can deduce an important observable: the kinetic energy distribution. This may allow us to distinguish the scission neutrons from the neutrons evaporated from fully accelerated fragments.

In sect. 2 the single-particle WFs and their FTs are introduced. Section 3 contains the sequence of necessary formulae to calculate the FTs in cylindrical coordinates. The formalism is tested in sect. 4 with a simple nuclear

[a] e-mail: rizea@theory.nipne.ro

potential that has an easy-to-predict momentum distribution. Section 5 contains the cases of more realistic potentials: spherical and deformed Woods-Saxon. The summary and conclusions are found in sect. 6.

2 Single-particle WFs and their FTs

In the independent-particle shell model, both for spherical [5] and for deformed [6] nuclei, the nucleonic wave functions $\Psi(\vec{r})$ are solutions of the Schrödinger equation (eigenfunctions of the single-particle Hamiltonian) with an average local potential (mean field) that is supposed to be created by the interaction with all other nucleons. These states are discrete and have well-defined energies. They are usually given in the position space and provide the probability in this space. If we want the probability in the momentum space *i.e.*, the probability that the nucleon has its momentum $\vec{p}$ in the volume element $\mathrm{d}^3\vec{p}$ we need to calculate the Fourier transform $\Phi(\vec{p})$ of $\Psi(\vec{r})$:

$$\Phi(\vec{k}) = \frac{1}{(2\pi)^{3/2}} \int_{-\infty}^{\infty} \Psi(\vec{r}) \mathrm{e}^{-\mathrm{i}\vec{k}\vec{r}} \mathrm{d}^3\vec{r}, \tag{1}$$

with $\vec{k} = \vec{p}/\hbar$. This is how the momentum representation is related to the space representation and viceversa:

$$\Psi(\vec{r}) = \frac{1}{(2\pi)^{3/2}} \int_{-\infty}^{\infty} \Phi(\vec{k}) \mathrm{e}^{\mathrm{i}\vec{k}\vec{r}} \mathrm{d}^3\vec{k}. \tag{2}$$

It is known that $\Psi(\vec{r})$ and $\Phi(\vec{k})$ are equaly valid descriptions of the state of the particle [7]. They are however not generally equivalent when viewed as square integrable functions.

3 Two-dimensional Fourier transform

We start with the standard form of the Fourier transform in Cartesian coordinates:

$$F(u,v) = \hat{f}(u,v) = \int_{-\infty}^{+\infty} \int_{-\infty}^{+\infty} f(x,y) \mathrm{e}^{-2\pi\mathrm{i}(xu+yv)} \mathrm{d}x\, \mathrm{d}y. \tag{3}$$

Let's introduce the polar coordinates (ρ, θ):

$$x = \rho\cos\theta, \qquad y = \rho\sin\theta$$

and their conjugates (R, ϕ):

$$u = R\cos\phi, \qquad v = R\sin\phi.$$

From (3) we obtain the Fourier transform in polar coordinates:

$$F(R,\phi) = \int_0^{2\pi} \int_0^{\infty} f(\rho,\theta) \mathrm{e}^{-2\pi\mathrm{i}\rho R\cos(\theta-\phi)} \rho \mathrm{d}\rho\, \mathrm{d}\theta. \tag{4}$$

When the function f is *radial* (or *axially symmetric*), *i.e.* it depends only on ρ, not on θ, the transform (4) takes the form:

$$F(R) = 2\pi \int_0^{\infty} f(\rho) J_0(2\pi\rho R) \rho \mathrm{d}\rho, \tag{5}$$

where J_0 is the zero-order Bessel function of the first kind. Note that the Fourier transform of a radial function is also radial. The formula for $F(R)$ in terms of $f(\rho)$ is called the zero-order Hankel transform or the Fourier-Bessel transform.

For the relation to the form used in quantum mechanics see the appendix. Note here that $u = k_x/(2\pi)$, $v = k_y/(2\pi)$, $R = k_\rho/(2\pi)$. The variables x, y, ρ belong to the position space, while u, v, R, k_x, k_y, k_ρ belong to the momentum space. The factor $1/2\pi$ is introduced as a phase convention.

If we have a function in cylindrical coordinates, which does not depend on the angles ϕ and θ, its Fourier transform will be

$$F(R,Z) = \\ 2\pi \int_{-\infty}^{\infty} \left[\int_0^{\infty} f(\rho,z) J_0(2\pi\rho R) \rho \mathrm{d}\rho \right] \mathrm{e}^{-2\pi\mathrm{i}zZ} \mathrm{d}z, \tag{6}$$

where $Z = k_z/(2\pi)$ according to the relation with the quantum mechanics variables.

Thus, the Fourier transform in cylindrical coordinates implies a combination of one-dimensional Fourier and Hankel transforms. Let us note that according to Parseval's theorem, the Fourier transform has the property of norm conservation.

Suppose now that the function $f(\rho, z)$ is known only on the nodes of a discrete grid. Then, the Fourier transform will be also a discrete function, approximation of the continuous transform. Let $\rho_j = \rho_0 + j\Delta\rho$, $j = 0, 1, \ldots, M-1$ and $z_k = z_0 + k\Delta z$, $k = 0, 1, \ldots, N-1$ be the points (uniformly spaced) defining the grid for which $f(\rho_j, z_k)$ are given. The interval $[\rho_0, \rho_{M-1}]$ is a subinterval of $[0, \infty[$, while the interval $[z_0, z_{N-1}]$ is a subinterval of $]-\infty, +\infty[$. The function $f(\rho, z)$ is zero for $\rho > \rho_{M-1}$, $z < z_0$ and $z > z_{N-1}$.

We shall treat separately the two implied integrals.

3.1 Hankel transform

Let us consider the integral

$$H(R,z) = 2\pi \int_0^{\infty} f(\rho,z) J_0(2\pi\rho R) \rho \mathrm{d}\rho. \tag{7}$$

For a position $z = z_k$, since f is zero beyond ρ_{M-1}, one has

$$H(R,z) \approx 2\pi \int_{\rho_0}^{\rho_{M-1}} f(\rho,z) J_0(2\pi\rho R) \rho \mathrm{d}\rho.$$

Note that in principle $\rho_0 = 0$. In the examples given below (in sects. 4 and 5) $\rho_0 > 0$, but the value at $\rho = 0$

is obtained by extrapolation (see sect. 4.1). The integral on the whole interval $[\rho_0, \rho_{M-1}]$ is represented as a sum of integrals on intervals of the size $2\Delta\rho$. To approximate these partial integrals (denoted by I_j) we have deduced a quadrature formula of the form

$$I_j \approx \alpha f(\rho_j, z) + \beta f(\rho_{j+1}, z) + \gamma f(\rho_{j+2}, z), \qquad (8)$$

which is exact when f (as a function of ρ) is a polynomial of degree at most 2. Such a formula is similar to Filon's rule for integrals of the form $\int_a^b f(x)w(\omega x)\mathrm{d}x$ (w = sin or cos), but adapted for Bessel instead of trigonometric functions.

In order to obtain the coefficients α, β, γ we replace in (8) the function $f(\rho, z)$ by 1, ρ, ρ^2 successively and use analytical expressions for integrals of the type

$$\int_{\rho_j}^{\rho_{j+2}} \rho^p J_0(2\pi\rho R)\mathrm{d}\rho, \quad p = 1, 2, 3.$$

The corresponding primitives are expressed in terms of Bessel functions J_0, J_1 and of Struve functions H_0, H_1 (see [8]). In order to compute the Bessel functions we have used the subroutine REALJN from the Computer Physics Communications Program Library [9]. The Struve functions are calculated by the subroutines STRVH0 and STRVH1 from the package 757 of the TOMS library [10].

The Fourier transform will be also calculated on a discrete grid defined by the points R_m and Z_n (see sects. 3.2 and 4.1). If the transforms of several functions are to be obtained, the Bessel and Struve functions should be calculated once at the points corresponding to each pair (ρ_j, R_m) and stored in the memory.

We note that many papers have been devoted to the numerical evaluation of the Hankel transform. The oscillatory behaviour of the Bessel function and the infinity in the integration range make the computation of this transform difficult. Different techniques have been proposed in the past. We cite some representative articles: *i.e.* [11], [12], [13], [14]. Generally, these procedures assume an analytical form of the initial function. Since our functions are usually known only on a discrete grid, we derived a computation method suited for such a case. Tested on different exact examples, the method has proven to be quite efficient in terms of rapidity and accuracy.

3.2 Discrete Fourier transform

For any R_m from the discrete grid, let us consider the integral

$$F(R_m, Z) = \int_{-\infty}^{\infty} H(R_m, z)\mathrm{e}^{-2\pi\mathrm{i}zZ}\mathrm{d}z. \qquad (9)$$

The variable Z takes a set of N values defined as

$$Z_n = \frac{n - N/2}{N\Delta z}, \quad n = 0, 1, \ldots, N-1.$$

Equation (9), evaluated at the point Z_n is approximated by

$$\begin{aligned} F(R_m, Z_n) &\approx \Delta z \sum_{k=0}^{N-1} H(R_m, z_k)\mathrm{e}^{-2\pi\mathrm{i}z_k Z_n} \\ &= \Delta z \sum_{k=0}^{N-1} H(R_m, z_k)\mathrm{e}^{-2\pi\mathrm{i}(z_0 + k\Delta z)Z_n} \\ &= \Delta z \mathrm{e}^{-2\pi\mathrm{i}z_0 Z_n} \sum_{k=0}^{N-1} H(R_m, z_k)\mathrm{e}^{-2\pi\mathrm{i}(k\Delta z)Z_n}. \end{aligned} \qquad (10)$$

Taking into account the definition of Z_n, we have

$$\begin{aligned} \mathrm{e}^{-2\pi\mathrm{i}(k\Delta z)Z_n} &= \mathrm{e}^{-2\pi\mathrm{i}(k\Delta z)\left(\frac{n}{N} - \frac{1}{2}\right)/\Delta z} \\ &= \mathrm{e}^{k\pi\mathrm{i}}\mathrm{e}^{-2\pi\mathrm{i}(kn)/N} = (-1)^k \mathrm{e}^{-2\pi\mathrm{i}(kn)/N}. \end{aligned}$$

Thus, the approximation (10) becomes

$$F(R_m, Z_n) \approx \Delta z \mathrm{e}^{-2\pi\mathrm{i}z_0 Z_n} \sum_{k=0}^{N-1} (-1)^k H(R_m, z_k)\mathrm{e}^{-2\pi\mathrm{i}(kn)/N}. \qquad (11)$$

For a given set g_k, $k = 0, 1, \ldots, N-1$ the set of the N following values

$$G_n = \sum_{k=0}^{N-1} g_k \mathrm{e}^{-2\pi\mathrm{i}(kn)/N}, \quad n = 0, 1, \ldots, N-1 \qquad (12)$$

is called the *discrete Fourier transform*.

Comparing eqs. (11) and (12), we can write the relation

$$F(R_m, Z_n) \approx \Delta z \mathrm{e}^{-2\pi\mathrm{i}z_0 Z_n} G_n, \qquad (13)$$

where $g_k = (-1)^k H(R_m, z_k)$.

An efficient way of calculating G_n values is to use a special algorithm named the *fast Fourier transform* (FFT). It requires N to be a power of 2. The literature on this subject is vast. We cite for example the comprehensive treatise of Briggs and Henson [15]. In our calculation we have used the subroutine FOURN from *Numerical Recipes* [16], based on the FFT algorithm.

In conclusion, to obtain the values $F(R_m, Z_n)$ representing the discrete Fourier transform in cylindrical coordinates, we first apply the discrete Hankel transform to get $H(R_m, z_k)$ and then the discrete Fourier transform in one dimension (the z-axis).

4 A simple case

We start with a test example that is expected to have a simple momentum (kinetic energy) distribution: a spherical nucleus with sharp surface and no spin-orbit coupling filled with independent neutrons that have zero orbital angular momentum. The potential inside the nucleus is uniformly constant, see fig. 1. The momentum of each neutron state has, in classical mechanics, a unique value. In quantum mechanics we expect, instead of a δ-function, a distribution of momenta which, however, should still keep a simple shape.

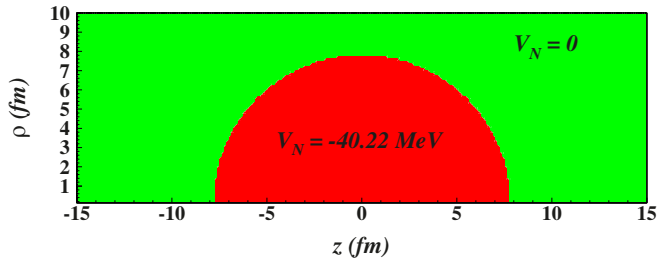

Fig. 1. A spherical well with constant depth used as a test example.

4.1 Eigenfunctions and their Fourier transforms

We therefore consider the following eigenvalue problem in cylindrical coordinates

$$Hf_i(\rho,z) = E_i f_i(\rho,z) \tag{14}$$

of the following single-particle Hamiltonian:

$$H = -\frac{\hbar^2}{2\mu}\left[\frac{1}{\rho}\frac{\partial}{\partial\rho} + \frac{\partial^2}{\partial\rho^2} + \frac{\partial^2}{\partial z^2} - \frac{\Lambda^2}{\rho^2}\right] + V(\rho,z).$$

Λ is the projection of the orbital angular momentum on the symmetry axis and $V(\rho,z)$ is the potential. It has the constant value -40.22 MeV inside a semi-circular domain and 0 outside. The radius of the domain is equal to the nuclear radius $r_0 A^{1/3}$, with $r_0 = 1.347$ fm. By the function change $g_i = \sqrt{\rho} f_i$, the first derivative from H is removed, resulting in a simplified Hamiltonian $\hat{H}$ of the form

$$\hat{H} = -\frac{\hbar^2}{2\mu}\left[\frac{\partial^2}{\partial\rho^2} + \frac{\partial^2}{\partial z^2} - \frac{\Lambda^2 - 1/4}{\rho^2}\right] + V(\rho,z),$$

and the problem (14) becomes equivalent to

$$\hat{H} g_i = E_i g_i. \tag{15}$$

Note that the Hamiltonian $\hat{H}$ is self-adjoint for null boundary conditions (corresponding to bound states), so that its spectrum is real (see [17]). The corresponding eigenfunctions are continuous, the singularity of the potential introducing discontinuities only in the g_i second-order derivatives (at the edge of the potential well). After obtaining g_i, the original function f_i is recovered from $f_i = g_i/\sqrt{\rho}$.

To solve (15) the infinite physical domain is limited to a finite one, which is discretized by a grid with the mesh points $\rho_j = \rho_0 + j\Delta\rho$, $j = 0,1,\ldots,M-1$ and $z_k = z_0 + k\Delta z$, $k = 0,1,\ldots,N-1$. In the present calculations we have used a step $h = \Delta\rho = \Delta z = 1/16$ fm. The numbers of the grid points are $M = 256$ and $N = 512$, while $\rho_0 = \Delta\rho$ and $z_0 = -16$ fm. At each point the partial derivatives in $\hat{H}$ are approximated by finite difference formulas. For the derivatives with respect to z we use the standard 3-point formula, while for the derivatives in ρ, we use a special formula, which takes into account the accomplished function transformation [18]. The eigenvalue problem (15) is transformed into an algebraic eigenvalue problem with a large sparse matrix, which is solved by the package ARPACK, based on the implicitly restarted Arnoldi method [19]. The resulting eigenfunctions are ortho-normalized by the Gram-Schmidt procedure. The values at $\rho = 0$ have been obtained by extrapolation, since $f_i(0,z)$ cannot be deduced from g_i for these points.

In order to compute the Hankel-Fourier transform, the grid is first extended so that $M = 1024$, $N = 2048$, $\rho_0 = 0$, $z_0 = -64$ fm, keeping the same steps $\Delta\rho$ and Δz. A better FT resolution is thus allowed. The eigenfunction values are placed in the corresponding points, the rest of the grid being filled with zeros. The function values towards the limits of the original grid are exponentially decreasing (up to 10^{-5}) and the discontinuity is not expected to influence the results presented here. The grid of the transform is defined by

$$R_m = R_0 + m\Delta R,\ R_0 = 0,\ m = 0,1,\ldots,M-1,\ \Delta R = \frac{1}{256}$$

and

$$\begin{aligned} Z_n &= \frac{n - N/2}{N\Delta z} = Z_0 + n\Delta Z, \\ Z_0 &= -8, \quad n = 0,1,\ldots,N-1, \\ \Delta Z &= \frac{1}{N\Delta z} = \frac{1}{128}. \end{aligned}$$

The units for Z_0 and ΔZ are fm^{-1}.

So, we have ensured a sufficiently large range of the transform, as well as a power of 2 for the number of points on Z-axis, allowing the use of the FFT algorithm.

As a test of accuracy, we have checked out the norm conservation. An error estimate was formed by

$$\epsilon_{FHT} = \frac{1}{N_e}\sum_{i=1}^{N_e} |\|F_i\| - \|f_i\||,$$

where N_e is the number of eigenstates, f_i is the initial function (its norm is equal to 1) and F_i is the transformed function. The norms are defined by

$$\|f\| = 2\pi\int_{-\infty}^{\infty}\int_0^{\infty} \rho\,|f(\rho,z)|^2 \mathrm{d}\rho\mathrm{d}z$$

and

$$\|F\| = 2\pi\int_{-\infty}^{\infty}\int_0^{\infty} R\,|F(R,Z)|^2 \mathrm{d}R\mathrm{d}Z$$

For the case of the nucleus ^{236}U and $\Lambda = 0$ there are 15 eigenstates with negative energies.

After computing all 15 transforms, we have found the following value for ϵ_{FHT} (the mean error):

$$\epsilon_{FHT} = 4.32 \times 10^{-7}.$$

This shows that the transforms preserve the norm with an accuracy of about 7 digits. All calculations have been performed in double-precision arithmetic. The integrals

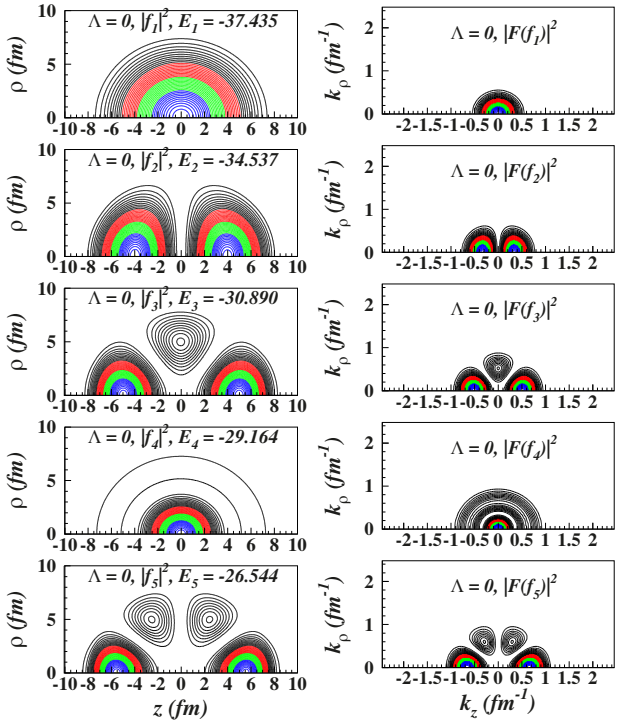

Fig. 2. WFs 1 to 5 and the corresponding FTs.

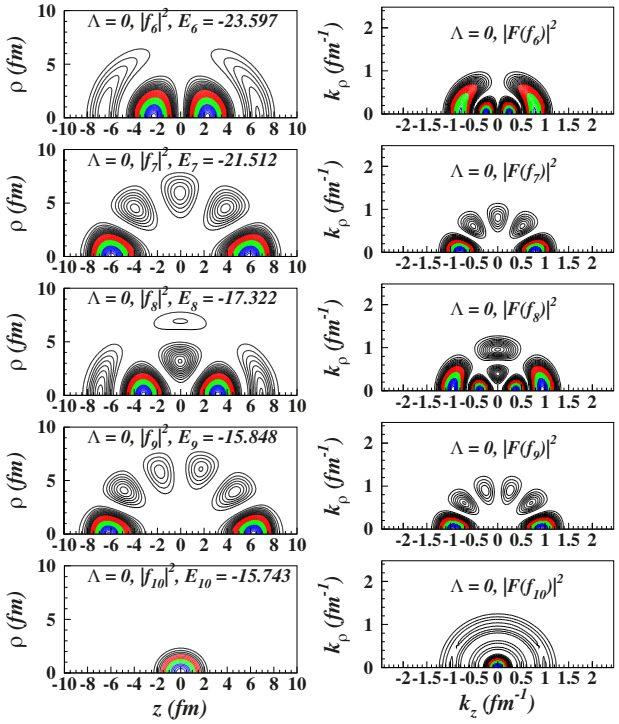

Fig. 3. WFs 6 to 10 and the corresponding FTs.

giving the norms have been calculated by a Newton-Cotes formula [20] extended to two dimensions.

The corresponding neutron wave functions $f_i(\rho, z)$ are shown (as squared moduli) on the left of figs. 2, 3, 4. Their Fourier transforms $F_i(k_\rho, k_z)$ are shown for comparison (also as squared moduli) on the right of the same figures ($k_\rho = 2\pi R$, $k_z = 2\pi Z$, see the appendix). The apparent similarity of the shapes of the original functions and of their Fourier transforms immediately attracts the attention. This result is unusual since among all elementary functions only a Gaussian has a Gaussian as Fourier transform. These shapes resemble only for $\Lambda = 0$ states (which have no centrifugal potential) but even in this case they are not identical. This can be seen in figs. 5 and 6 where a detailed comparison of selected functions and their transforms is shown for slices along the z- and ρ-axes, respectively. Among the cases represented, only the wave function number 10 and its Fourier transform are very similar along both axes. In general, the FTs show a more intense last oscillation than the WFs. It is interesting to note that the FT has the same number of nodes as the WF in both directions; only their amplitudes vary.

One can conclude that the apparent similarities between the WFs and the FTs are mainly due to the conservation of the number of nodes but also to the bidimensional representation chosen in figs. 2 to 4 which seems to disguise the results.

Due to the Heisenberg uncertainty principle, the neutron momentum cannot have a well-defined value. It has a distribution instead. Examining the contour maps in fig. 2 (right) one perceives a circle on which the peaks of FT lay but also large uncertainties around this most probable value. One can anticipate that the neutron will not have a precise kinetic energy as in a classical well of constant depth.

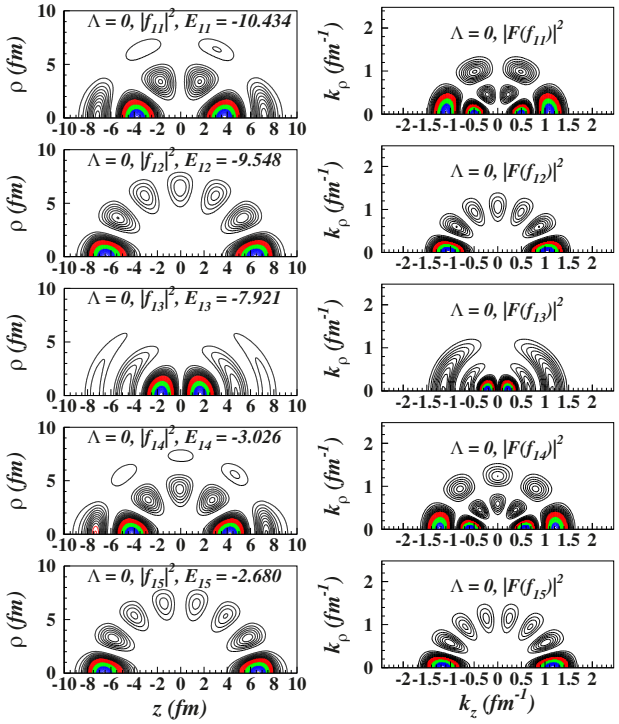

Fig. 4. WFs 11 to 15 and the corresponding FTs.

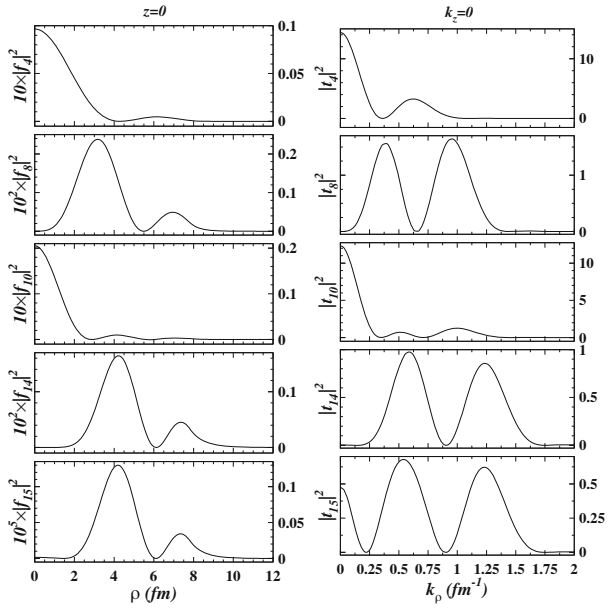

Fig. 5. $|WF|^2$ 4, 8, 10, 14, 15 and the corresponding $|FT|^2$ at $z = 0$.

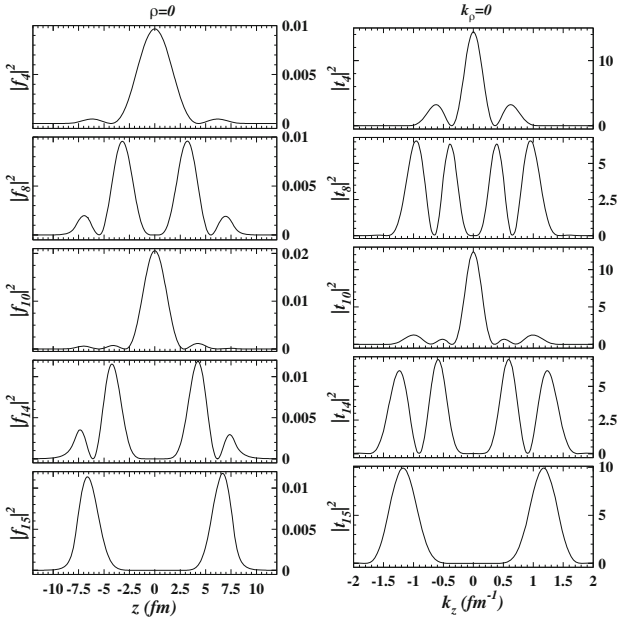

Fig. 6. $|WF|^2$ 4, 8, 10, 14, 15 and the corresponding $|FT|^2$ at $\rho = 0$.

4.2 Momentum distributions

Points in the (k_ρ, k_z)-plane having the same modulus $K = \sqrt{k_\rho^2 + k_z^2}$ form a circle. The total probability that a measurement of the neutron momentum gives the result K is the sum of the contributions from all the points of this circle.

The probability to find the neutron momentum in a given element is

$$P_{k_\rho,k_z} = |F(k_\rho, k_z)|^2 k_\rho \Delta k_\rho \Delta k_z. \quad (16)$$

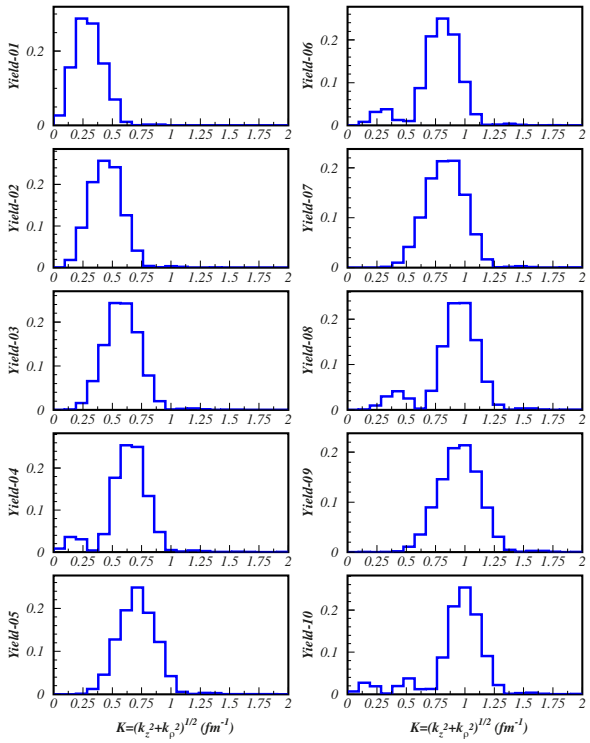

Fig. 7. The distribution of the modulus of the momentum K for the states 1 to 10.

Hence an absolute value K_{k_ρ,k_z} and a probability P_{k_ρ,k_z} are associated to each grid point. To represent the K-distributions as histograms, we divide the domain of K-values in equal intervals and group the points according to the interval to which they belong. Summing the probabilities of the points in each group one obtains the probability that a neutron has its K-value in the respective interval. The resulting histograms are shown in figs. 7, 8.

As expected, with increasing energy (*i.e.*, the index of the wave function) the K-distribution shifts to larger momenta. The width is however almost the same reflecting the confinement of the wave function inside the nucleus: each state practically occupies the whole nucleus. Hence a constant spread of the positions leads to a constant spread of the momenta (Heisenberg).

What is not expected from the analogy with the classical mechanics or from the uncertainty principle is that, for certain states, the K-distribution has more than one peak. This can be understood from figs. 2, 3 and 4. The maxima of the square modulus of the Fourier transform lie on circles on the (k_z, k_ρ)-plane. The number of nodes in the radial direction determines the number of such circles which in turn gives the number of the peaks. Therefore this unexpected feature is easy to explain using the present results.

One should stress that the clear correlation between the number of nodes of the WF and the number of peaks of the corresponding momentum distribution holds only for $\Lambda = 0$. The centrifugal term Λ^2/ρ^2 creates a turning point at small ρ values that reduces the range of the K values: more in the ρ-direction than in the z-direction.

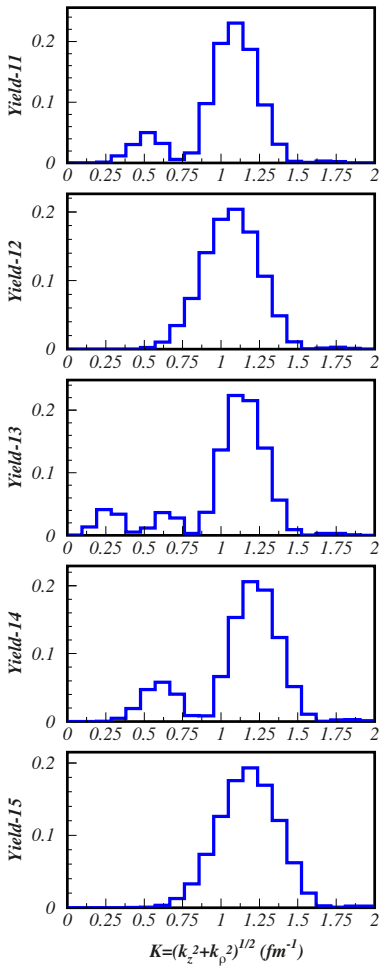

Fig. 8. The distribution of the modulus of the momentum K for the states 11 to 15.

This flattens the $|F(k_\rho, k_z)|^2$ distribution, moves the locus of the maxima away from a circle and broadens the peaks. As we will see in the next section a similar effect is produced by the nuclear deformation.

Finally, a discussion of the K-distribution of the lowest level ($E_1 = -37.44\,\mathrm{MeV}$) is instructive. Its kinetic energy, approximately $E_1 - V_N = 2.76\,\mathrm{MeV}$ should represent the minimum kinetic energy compatible with the uncertainty relation (the so-called "zero-point motion"). The average value $\langle K\rangle$ of the calculated distribution (see upper-left frame of fig. 7) is $0.35\,\mathrm{fm}^{-1}$ corresponding to a kinetic energy $E_{\mathrm{kin}} = \frac{\hbar^2}{2\mu}\langle K^2\rangle = 2.55\,\mathrm{MeV}$; hence in good agreement with the value from above. It appears that this constraint imposed by Heisenberg's principle should be understood only in terms of average values. Since the K-distribution is quite large, a measurement of the momentum can lead to smaller values.

Small differences between the present calculations and the predictions of classical mechanics are also due to the fact that the WF (contrary to the classical particle) extends beyond the wall of the potential. The evanescent parts of the WF tend, *e.g.*, to slightly diminish E_{kin} as in the comparison from above (2.55 MeV instead of 2.76 MeV). It increases the average potential energy $\langle f_i|V_N|f_i\rangle$ since the integration is performed also over a small domain where $V_N = 0$ instead of $-40.22\,\mathrm{MeV}$.

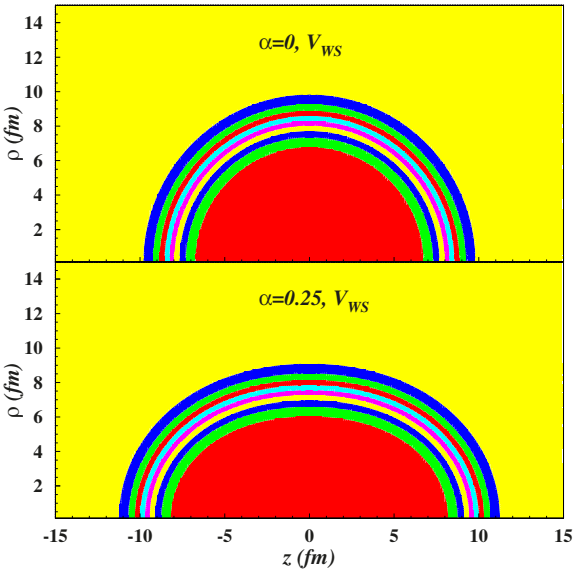

Fig. 9. A spherical and a deformed Woods-Saxon potential (used as realistic examples).

5 A realistic potential

After this pedagogical example we study, in this section, a more realistic neutron-nucleus potential. It is of Woods-Saxon type (hence diffuse surface) and contains a spin-orbit term [21, 22]. The nuclear shape is described by a Cassinian oval with a given deformation parameter α [23]. Calculations are performed for a spherical ($\alpha = 0$) and for a deformed ($\alpha = 0.25$) ^{236}U nucleus. The corresponding potentials are represented in fig. 9.

Due to the spin-orbit coupling the wave functions have two components corresponding to spin "up" and spin "down". For a given projection Ω of the total angular momentum on the symmetry axis they assume the form

$$|\Psi_j\rangle = f_j^{(1)}(\rho, z)\mathrm{e}^{\mathrm{i}\Lambda_1\theta}|\uparrow\rangle + f_j^{(2)}(\rho, z)\mathrm{e}^{\mathrm{i}\Lambda_2\theta}|\downarrow\rangle. \qquad (17)$$

The values Λ_1, Λ_2 are defined by

$$\Lambda_1 = \Omega - \frac{1}{2}\,, \qquad \Lambda_2 = \Omega + \frac{1}{2}\,,$$

Ω is a good quantum number. Because of the left-right symmetry, the parity π is also conserved.

Be $|\Psi_j\uparrow|^2$ and $|\Psi_j\downarrow|^2$ the square moduli of the two components after integration over θ. Their sum gives the square modulus of the whole WF. The Fourier transform of (17) is calculated for each component separately. Be $|F\Psi_j\uparrow|^2$ and $|F\Psi_j\downarrow|^2$ the square moduli of the same quantities but for their Fourier transform. Their sum gives the square modulus of the whole FT.

These quantities are represented, for a spherical nucleus, in fig. 10 for selected WFs with $\Omega = 1/2$ and for

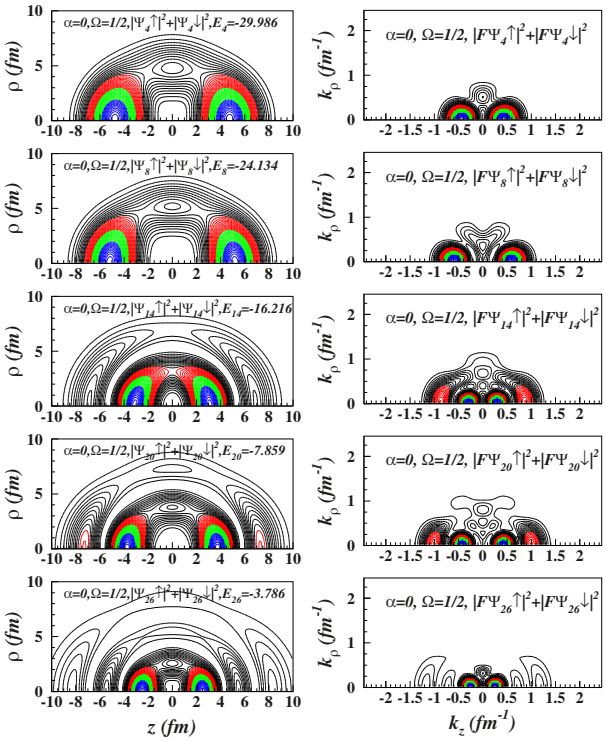

Fig. 10. Square moduli of selected WFs (left) and of the corresponding FTs (right) for spherical ($\alpha = 0$) Woods-Saxon potential.

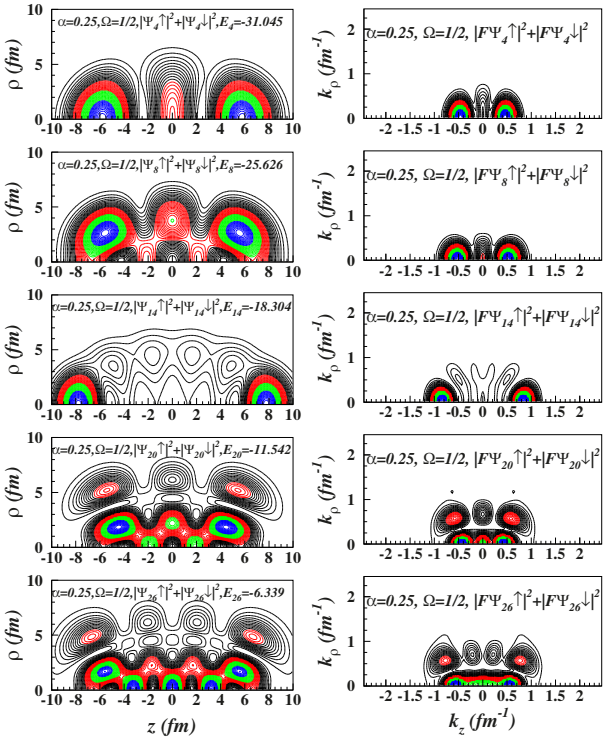

Fig. 11. Square moduli of selected WFs and of the corresponding FTs for deformed ($\alpha = 0.25$) Woods-Saxon potential.

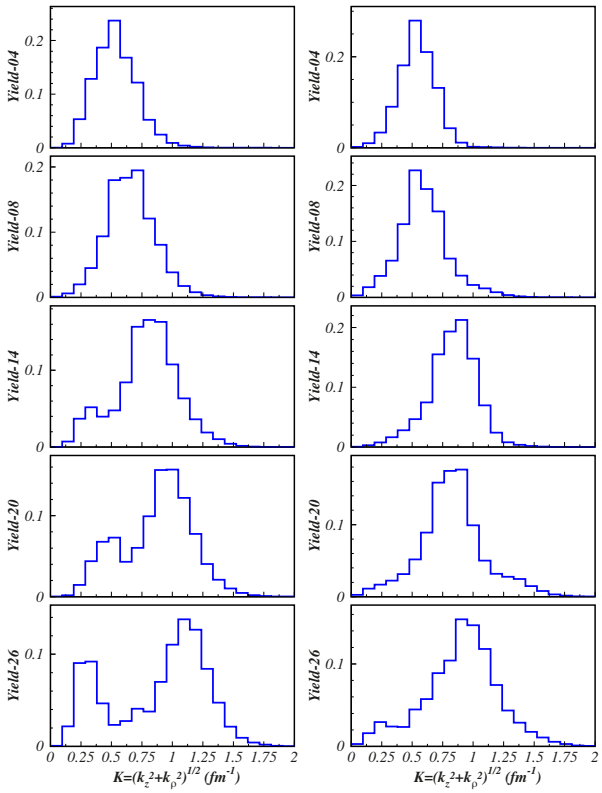

Fig. 12. The distribution of the modulus of the momentum K for selected states: $\alpha = 0$ (left) and $\alpha = 0.25$ (right).

the corresponding FTs. As compared with the results from figs. 2 to 4 there is still some resemblance between the WFs and their FTs. We stressed in sect. 4.1 that similarity occurs only for $\Lambda = 0$ states. Since now the WFs contain a mixture of $\Lambda = 0$ and 1 states, a certain loss of resemblance is understandable. For states with higher Ω values the resemblance is even expected to disappear. For the same reason these bidimensional plots are more complex than in the simple case and the circular ridges in the FT plots are less pronounced. As expected, for a deformed nucleus (fig. 11) the same reduction of the similarity between the WFs and their FTs is observed with this time an increase in complexity. There is however a noticeable difference: the ridge of the square modulus of FT is no more a circle but an ellipse. Hence the ridge does not coincide anymore with the locus of a constant K value. As compared with the spherical case, one can foresee a single-peaked, somewhat wider K-distribution.

Using $|F(k_\rho, k_z)|^2 k_\rho \Delta k_\rho \Delta k_z$, one can construct, as before, a histogram with the moduli K. The results are presented in fig. 12 for a spherical (left) and for a deformed (right) nucleus. Even if, as in the simple case, the location of the maximum shifts towards larger values with increasing the energy of the state, very low momenta (down to zero) are always populated. The combined effect is an increase in the width of the K-distribution. The analogy with classical mechanics can provide an explanation: in a diffuse potential a particle has a continuous distribution of momenta from zero (at the turning point, on the po-

tential edge) to a maximum value (at the bottom of the potential well).

Since, in a deformed nucleus, the K values along the ridge of the square modulus of FT are no more constant, the K-distribution has only one broad peak. The effect of nuclear deformation on the momentum distributions is therefore non-negligible and has to be taken into account in the analyses of experimental data obtained in direct reactions with deformed nuclei.

6 Summary and conclusions

In direct nuclear reaction theories, the removal of the nucleon is treated in the sudden approximation, *i.e.*, the nucleon is supposed to retain the properties (*i.e.*, quantum numbers) of the bound state from which it was ejected. The calculations of the momentum distribution of the ejected nucleon (which is an observable) involves the Fourier transform of the corresponding nucleonic wave function. In the case of a deformed nucleus this wave function is usually expressed in cylindrical coordinates. The Fourier transforms of such wave functions are therefore necessary. To our knowledge, the present study contains the first calculations of this type in nuclear structure. The formalism and the computing approach used are described in details. The FT of a nucleonic WF leads directly to the distribution of the linear momenta of the respective nucleon.

The first potential (a well with sharp walls and of a constant depth) is chosen because a classical particle moving in it has the simplest possible momentum distribution (a δ-function). Due to the uncertainty relation, the corresponding distribution of a quantum particle is expected to be wide and single-peaked. We have found that the calculated distribution, in addition of being wider, has from one to three peaks, depending on the number of nodes of the WF. The explanation is that the FT conserves the number of nodes of the WF and therefore the square modulus of the FT can exhibit more than one spherical ridge naturally leading to multiple-peaked K-distributions.

The second choice is a Woods-Saxon potential that is known to describe realistically a spherical nucleus. Due to its diffuseness, a classical particle has a continous momentum distribution that stretches from the origin up to a maximum value. As a result, in addition to the abovementioned peaks, wider this time, the K-distribution of a nucleon exhibits a tail towards $K = 0$ and a less pronounced structure.

The third choice is a deformed Woods-Saxon potential. The ridges of the square modulus of the FT are no more spherical but ellipsoidal. They no more coincide with the geometrical locus of constant K values which is still a circle. Along these ridges the K value varies and, consequently, the structures are washed out. A measurable difference between the momentum distributions of nucleons in spherical and deformed nuclei is therefore predicted.

We may conclude that the present study encourages new experimental investigations of direct reactions involving both spherical and deformed heavy nuclei. From the theoretical side the effect of a further increase of the nuclear deformation (*i.e.*, along the fission path) on the momentum distribution should be estimated. New interesting aspects are expected to be found.

Appendix A.

Let us consider the one-dimensional Fourier transform in quantum mechanics:

$$F_1(k) = \frac{1}{\sqrt{2\pi}} \int_{-\infty}^{\infty} f(x) \mathrm{e}^{-\mathrm{i}kx} \mathrm{d}x. \tag{A.1}$$

The variable x belongs to the position space and the variable k belongs to the momentum space.

In order to deduce the relation with the standard transform:

$$F(\omega) = \int_{-\infty}^{\infty} f(t) \mathrm{e}^{-\mathrm{i}2\pi t\omega} \mathrm{d}t$$

let us make the notations $k = \sqrt{2\pi}U$, $x = \sqrt{2\pi}u$. We have

$$\begin{aligned} F_1\left(\sqrt{2\pi}U\right) &= \frac{1}{\sqrt{2\pi}} \int_{-\infty}^{\infty} f\left(\sqrt{2\pi}u\right) \mathrm{e}^{-\mathrm{i}2\pi uU} \sqrt{2\pi} \mathrm{d}u \\ &= \int_{-\infty}^{\infty} f\left(\sqrt{2\pi}u\right) \mathrm{e}^{-\mathrm{i}2\pi uU} \mathrm{d}u. \end{aligned}$$

With the change of variable $t = \sqrt{2\pi}u$, the last integral becomes:

$$\frac{1}{\sqrt{2\pi}} \int_{-\infty}^{\infty} f(t) \mathrm{e}^{-\mathrm{i}2\pi tU/\sqrt{2\pi}} \mathrm{d}t$$

so that

$$F_1(\sqrt{2\pi}U) = \frac{1}{\sqrt{2\pi}} F\left(\frac{U}{\sqrt{2\pi}}\right).$$

Denoting $U = \sqrt{2\pi}\omega$ we have

$$F_1(2\pi\omega) = \frac{1}{\sqrt{2\pi}} F(\omega)$$

or

$$F_1(k) = \frac{1}{\sqrt{2\pi}} F(\omega) \tag{A.2}$$

if $k = 2\pi\omega$. Thus, to obtain the Fourier transform in variable k one has to multiply the standard transform by $\frac{1}{\sqrt{2\pi}}$. In two dimensions, the factor will be $\frac{1}{2\pi}$. The variables of the two transforms differ by a factor of 2π.

Work partially supported by UEFISCDI Romania under the program PNII, contract no. 116/05.10.2011 and by PN 16 42 01 01/2016 of the Romanian Ministry of National Education and Scientific Research.

References

1. M.K. Banerjee, in *Nuclear Spectroscopy*, edited by Fay Ajzenberg-Selove (Academic Press, New York, London, 1960) Chapt. 2, p. 695.
2. P.G. Hansen, J.A. Tostevin, Annu. Rev. Nucl. Part. Sci. **53**, 219 (2003).
3. C.A. Bertulani, P.G. Hansen, Phys. Rev. C **70**, 034609 (2004).
4. N. Carjan, M. Rizea, Phys. Lett. B **747**, 178 (2015).
5. M.G. Mayer, J.H.D. Jensen, *Elementary Theory of Nuclear Shell Structure* (Wiley, New York, 1955).
6. S.G. Nilsson, Mat. Fys. Medd. Dan. Vidensk. Selsk. **29**, 1 (1955) issue No. 1.
7. L.D. Landau, E.M. Lifshitz, *Quantum Mechanics* (Pergamon Press, Oxford, 1977).
8. W. Rosenheinrich, *Tables of Some Indefinite Integrals of Bessel Functions* (Jena, Germany, 2016) `www.eah-jena.de/~rsh/Forschung/Stoer/besint.pdf`.
9. J.P. Coleman, Comput. Phys. Commun. **21**, 109 (1980).
10. A.J. MacLeod, ACM Trans. Math. Softw. **22**, 288 (1996).
11. R. Piessens, Comput. Phys. Commun. **25**, 289 (1982).
12. V. Magni, G. Cerullo, S. DeSilvestri, J. Opt. Soc. Am. A **9**, 2031 (1992).
13. R. Barakat, B.H. Sandler, Comput. Math. Appl. **40**, 1037 (2000).
14. Rajesh K. Pandey, Vineet K. Singh, Om P. Singh, Commun. Comput. Phys. **8**, 351 (2010).
15. B. Briggs, E. Henson, *The FFT: An Owner's Manual for the Discrete Fourier Transform* (SIAM, Philadelphia, 1995).
16. W.H. Press, B.P. Flannery, S.A. Teukolsky, W.T. Vetterling, *Numerical Recipes* (Cambridge University Press, 1986) pp. 451–453.
17. M. Rizea, V. Ledoux, M. Van Daele, G. Vanden Berghe, N. Carjan, Comput. Phys. Commun. **179**, 466 (2008).
18. M. Rizea, N. Carjan, Commun. Comput. Phys. **9**, 917 (2011).
19. D. Sorensen, R. Lehoucq, Chao Yang, K. Maschhoff, `www.caam.rice.edu/software/ARPACK` (1996).
20. M. Abramowitz, I.A. Stegun, *Handbook of Mathematical Functions*, 8th ed. (Dover, New York, 1972) eq. 25.4.14, p. 886.
21. N. Carjan, M. Rizea, Phys. Rev. C **82**, 014617 (2010).
22. R. Capote, N. Carjan, S. Chiba, Phys. Rev. C **93**, 024609 (2016).
23. V. Pashkevich, Nucl. Phys. A **169**, 275 (1971).